Disassembly of a Core–Satellite Nanoassembled Substrate for Colorimetric Biomolecular Detection

John R. Waldeisen,[†,‡,§] Tim Wang,[‡,§] Benjamin M. Ross,[‡] and Luke P. Lee[†,‡,*]

[†]UC Berkeley/UCSF Graduate Program in Bioengineering and [‡]Department of Bioengineering, Biomolecular Nanotechnology Center, Berkeley Sensor and Actuator Center, University of California, Berkeley, California 94720, United States. [§]These authors contributed equally to this work.

ABSTRACT The disassembly of a core–satellite nanostructured substrate is presented as a colorimetric biosensor observable under dark-field illumination. The fabrication method described herein utilizes thiol-mediated adsorption and streptavidin–biotin binding to self-assemble core–satellite nanostructures with a sacrificial linking peptide. Biosensing functionality is demonstrated with the protease trypsin, and the optical properties of the nanoassemblies are characterized. A figure of merit is presented to determine the optimal core and satellite size for visual detection. Nanoassemblies with 50 nm cores and 30 or 50 nm satellites are superior as these structures achieve an orange to green color shift greater than 70 nm that is easily discernible by the naked eye. This colorimetric substrate may prove to be a favorable alternative to liquid-based colloidal sensors and a useful visual readout mechanism for point-of-care microfluidic diagnostic assays.

KEYWORDS: nanoparticle · colorimetric · biosensor · plasmonic · nanoassembly · core–satellite · self-assembly

The simultaneous realization of self-assembled colloidal gold nanocrystals by Mirkin and Alivisatos established a platform technology for "bottom up" fabrication that utilized fundamental principles from biology. The advent of this discovery has yielded a multitude of geometric nanoassembly variations such as lattice networks,[1,2] dimer and trimer configurations,[3–5] and core–satellite constructs.[5–11] These noble metal nanoassemblies have enabled optical investigations of plasmon resonance coupling[10,11] and the colorimetric detection of biological and chemical analytes such as single nucleotide polymorphisms (SNPs),[12] cocaine, adenosine,[13] lead,[14] caspase,[15] and rabbit IgG.[16] Such technologies may bolster the groundwork for a new generation of point-of-care (POC) diagnostic devices capable of identifying diverse analyte species, an improvement upon the commercially available immunoassay-based lateral flow test.[17] We propose an advancement upon the current suspension-based modality of colloidal biomolecular sensors that is better suited for on-chip diagnostic system integration while preserving the capability for diverse species detection. We present the fabrication of nanoassemblies constructed on a two-dimensional glass substrate, demonstrate the colorimetric functionality of biomolecular sensing *via* disassembly, and systematically analyze the optical detection properties of the substrate. Nanoconstructs with 50 nm cores and 30 or 50 nm satellites maximized the signal-to-noise ratio during biosensing and enabled visible colorimetric shifts from orange (>630 nm) to green (~560 nm) *via* the observation of scattered light with dark-field (DF) illumination.

The construction of colloidal gold biosensors using DNA, peptide, or aptamer linkers has enabled the detection of an assortment of species outside the typical antigen/antibody binding interactions observed in traditional immunoassays.[12–17] This method is advantageous as plasmonic nanoparticles are ~500 000 times more luminous than a fluorophore, have an unlimited photon budget, and do not bleach, blink, or require expensive spectroscopic equipment.[18] However, the technology to date has relied upon nanoconstructs suspended in solution. This assembly paradigm has five deficiencies that may be overcome by the use of disassembling nanostructures immobilized on a substrate. First, the sample analyte is diluted by at least 3 orders of magnitude when added to the suspension of nanostructures, diminishing detection limits. Second, impurities in the analyte such as salts and pH fluctuations might cause flocculation and subsequently a false positive readout. Third, the storage life is limited because suspended nanoparticles tend to aggregate and settle with time. Fourth, liquid-based assays are prone to containment issues such as spillage. Finally, fifth and arguably the most important fact is that previous liquid-based sensors rely upon changes in optical absorbance. Since the Beer–Lambert law states that absorbance has a linear

* Address correspondence to lplee@berkeley.edu.

Received for review January 22, 2011 and accepted June 6, 2011.

Published online June 13, 2011
10.1021/nn2002807

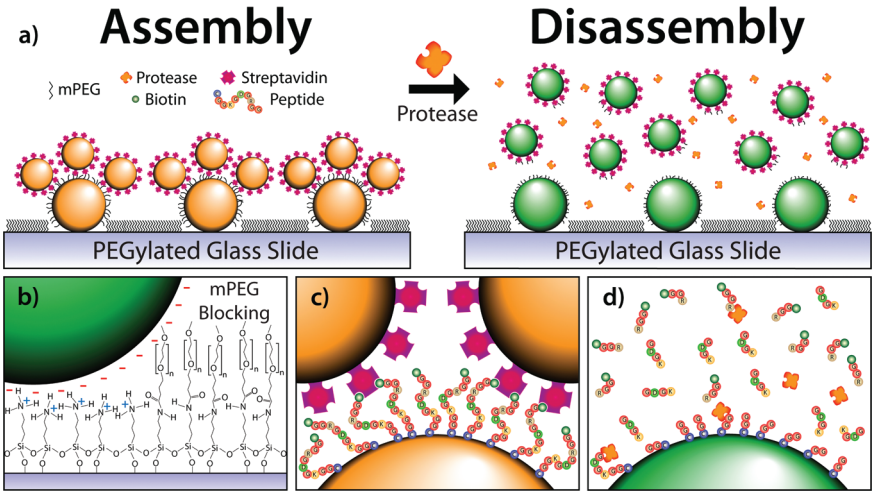

Figure 1. (a) Core–satellite Au nanoassemblies before and after proteolytic cleavage. (b) Immobilization of the negatively charged AuNP cores is enabled by Coulombic electrostatic attraction to an APTES monolayer on glass. The glass slide is subsequently passivated with an mPEG chain to block nonspecific satellite adsorption. (c) Satellite attachment is enabled by a directional cysteine/biotin–streptavidin peptide tether. (d) Addition of trypsin cleaves the peptide, releasing the satellites into solution and enabling colorimetric detection of the protease.

dependence on path length, colloidal liquid-based sensors are not feasible in microfluidic diagnostic systems. The colorimetric substrate presented here bypasses these shortcomings. Previous reports of disassembling colorimetric nanomaterials on a substrate have included the resuspension of nanoparticles released from nanolattices dried on hydrophobic paper or constructed on a fluid lipid bilayer membrane.[19,20] However, unlike previous biosensors, we present the first self-assembled substrate that yields a structural color change directly at the site of disassembly when imaged in DF. The small optical path length of the biosensing substrate (~nm) is better suited for the length scales of on-chip diagnostic systems in comparison to suspended nanoassembled networks that require longer path lengths (~cm) for colorimetric changes to be observable. The utility of this localized disassembly mechanism may enable functionality for spatiotemporal monitoring of cellular secretions and POC capability using innovative hand-held DF viewing techniques.

Protease diagnostics are greatly underutilized in clinical settings, thus a substrate able to detect protease activity was designed as a proof-of-concept to demonstrate the structurally induced spectral scattering shift of the biosensor. However, we stress that, by altering the core–satellite tether, detection platforms for other biomolecular species can be created. Detectable levels of proteases present in peripheral fluids taken *ex vivo* have been shown to act as diagnostic markers that are presymptomatically indicative of disease.[21–24] This article presents the use of scattered light from coupled gold nanoparticle assemblies and their subsequent disassembly *via* proteolysis as a colorimetric assay to detect protease activity. Cleavage of the nanoassemblies disengages the plasmon coupling between nanoparticles and shifts the observed DF scattered light from orange to green (Figure 1a). This model system not only is limited to protease activity monitoring but is applicable to the detection of numerous biomolecules.

RESULTS AND DISCUSSION

Gold nanoparticles (AuNPs) were first deposited onto APTES (3-aminopropyltriethoxysilane)-functionalized glass microscope slides. The sodium citrate reduction (Turkevich) method[25] produces negatively charged AuNPs, and the AuNPs, which served as the core of the nanoconstruct, were electrostatically immobilized onto the positively charged surface of the APTES glass slide through Coulombic attraction (Figure 1b, left). Next, a biotinylated 10 amino acid long peptide substrate, cleavable by the serine protease trypsin, was incubated on the substrate. The C-terminus of the peptide is a cysteine residue, enabling the thiol-mediated adsorption of the peptide onto the surface of the core nanoparticle. The peptide sequence is biotin-GGRGDGKGGC-OH. Streptavidin-conjugated satellite nanoparticles bind to the biotinylated N-terminus of the peptide for controlled, directional self-assembly (Figure 1c). The incubation of methoxy polyethylene glycol succinimidyl valerate (mPEG-SVA, M_W = 2 kDa) on the substrate before satellite deposition blocks the microscope slide such that the satellites only attach to the core nanoparticles. This essential step prevents the satellites from nonspecifically adsorbing onto the substrate and facilitates a reversible color shift. The APTES-functionalized slide enables passivation as the mPEG-SVA reacts with the exposed primary amine, releasing 1-hydroxy-2,5-pyrrolidinedione and immobilizing the PEG chain onto the slide (Figure 1b, right). It should be noted that the

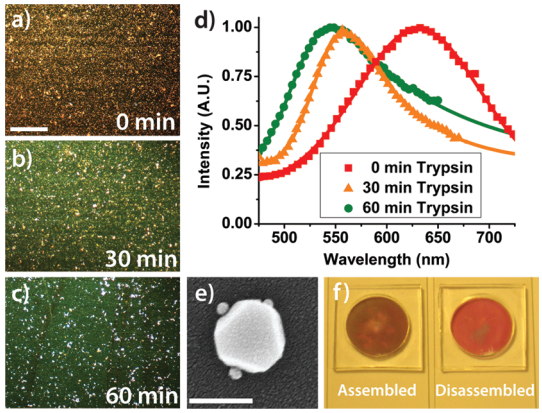

Figure 2. Dark-field microscopy images representative of the observable colorimetric shift upon disassembly by proteolytic cleavage with 100 μM trypsin at (a) 0 min, (b) 30 min, and (c) 60 min. The substrate is composed of 50 nm core AuNPs and 50 nm satellite AuNPs (scale bar = 100 μm). (d) Corresponding normalized spectra taken simultaneously with the images. (e) SEM image of an individual core–satellite nanoassembly with a 100 nm core and 10 nm satellites (scale bar = 100 nm), (f) A 50 nm core and 50 nm satellite nanoassembled substrate before and after trypsin cleavage *via* bright-field illumination. A colorimetric change is difficult to distinguish by eye as the short path length of the core–satellite nanoassembled substrate does not scatter enough of the incident light.

linking peptide chain could be replaced by a variety of other biomolecules such as an oligonucleotide or aptazyme for diverse analyte identification. All substrates were stored in deionized (DI) water to prevent capillary remodeling caused by evaporation. The substrates remained functional for more than 28 days when stored in DI water at 4 °C.

Pairs of slides were created for each geometrical combination of core and satellite size and analyzed under DF. A spectrophotometer measured the far-field scattering spectra from the substrate, and data taken from five random positions on each substrate were averaged to determine peak position and full width at half-maximum (FWHM). AuNP cores were deposited at high densities, ~33.1 cores μm^{-2} for 50 nm AuNP cores, enabling easy visualization of the scattered color, yet substrates were not overly dense, which would cause unfavorable plasmonic coupling between core particles. Four variations of core diameter were investigated. Thirty and 50 nm cores scattered green in comparison to 80 and 100 nm cores, which appeared chartreuse (Table S1 and Figure S1 in the Supporting Information). Additionally, the two larger core sizes have broader peak widths (FWHM). Radiation damping has been shown to be responsible for the red shift and bandwidth broadening observed in both the near- and far-field scattering as nanoparticles increase in size.[26] Core sizes with green scattering, which is the most sensitive color to the human eye, are optimal as their plasmon peak will be red-shifted upon satellite attachment and plasmon coupling. The red shift for assemblies with a large core size cannot be visually discerned as the far-field scattering spectra shift into the near-IR; however, such shifts are detectable with spectroscopy. Another important property for core size is the scattering cross section (σ_s). When a particle radius (r) is much smaller than the wavelength of light ($r \ll \lambda$), Rayleigh theory states $\sigma_s \propto r^6/\lambda^4$. Thus, core sizes of 30 nm and smaller have a small scattering cross section, resulting in dimly scattered green light which is difficult to visualize (Table S1 in the Supporting Information). The optimal core size, as determined by its spectral peak position and scattering cross section, is 50 nm.

The serine protease trypsin, known to cleave the carboxyl end of lysine and arginine, was used to initiate substrate disassembly (Figure 1d). Trypsin (100 μM) was spotted directly onto the substrate at room temperature (25 °C) and produced a complete color change in less than 40 min as seen in the images captured by a true-color charge-coupled device (CCD) camera (Figure 2). Panels a, b, and c of Figure 2 are time-lapse images of a substrate at 0, 30, and 60 min after trypsin exposure, respectively. The white spots observable in Figure 2c are believed to be scattering from mPEG-SVA aggregates that accumulated during surface passivation. A representative DF spectrum depicts a colorimetric shift greater than 70 nm for a substrate with 50 nm cores and 50 nm satellites (Figure 2d). Modified Gaussian curves have been fit to the data. An SEM image of a 100 nm core with 10 nm satellites is shown in Figure 2e. Core sizes larger than 100 nm scatter light greater than 600 nm, and satellite disassembly is visually indiscernible. Thus, larger sized core particles were eliminated from the study. A nanoassembled substrate with 50 nm cores and 50 nm satellites, before and after trypsin-mediated disassembly, is shown under bright-field illumination in Figure 2f. The short path length of the monolayer of core–satellites does not scatter enough of the incident light for a colorimetric change to be noticeably observable by eye. A technique similar to resonance-enhanced adsorption may be able to amplify this faint color shift under bright-field illumination and facilitate detection without the constraint of DF illumination.[27] Polydimethylsiloxane (PDMS) droplet immobilizers, visible in Figure 2f, were used to contain the droplet and prevent capillary-induced remodeling of the nanostructures due to evaporation. All of the images presented in Figure 2 are unaltered.

A large-scale study was performed for an array of nanostructures to characterize assembly and disassembly (Figure 3). Core sizes ranged from 30 to 100 nm, and satellite sizes ranged from 10 to 50 nm. Satellites larger than 50 nm are difficult to conjugate with streptavidin as the surface-to-volume ratio is large and the colloid becomes unstable during physio-adsorption of the streptavidin onto the AuNP surface. Substrates were prepared in duplicate, and optical measurements

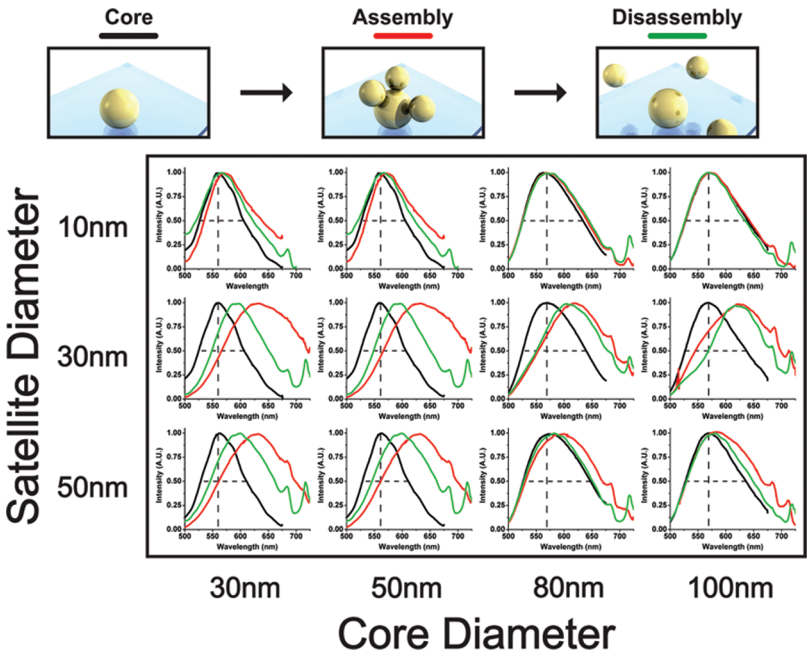

Figure 3. Spectral characterization study for a combination of core and satellite diameters. Scatter from single AuNP cores (black), assembly red shift (red), and disassembly blue shift (green) are depicted. Spectra are averaged results (n = 10). Core−satellite nanostructures with combinations of 30 and 50 nm nanoparticle sizes consistently produced the greatest peak shifts. Dashed black lines depict initial peak position and FWHM as a visual aid for the reader.

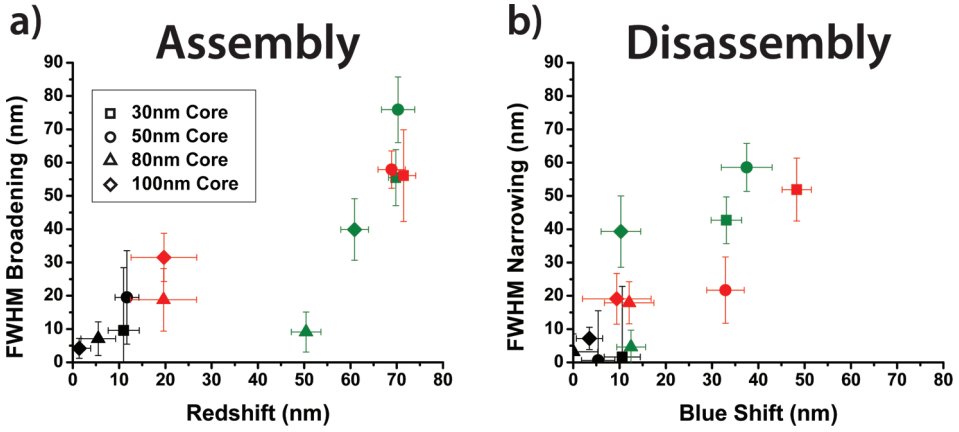

Figure 4. Correlation between peak shift and FWHM broadening/narrowing upon (a) assembly and (b) disassembly. Data points are extracted from Figure 3 with the shape corresponding to the core size and the color corresponding to the satellite size; 10, 30, and 50 nm satellites are represented by black, green, and red, respectively. The error bars represent sample standard deviation.

were acquired at random locations in quintuplicate for each slide (n = 10). The acquisitions were collected over a large field of view such that substrate inconsistencies and variations were averaged over the acquired spectrum. Disassembly was achieved by exposing the substrates to trypsin for 60 min at room temperature. The 10 spectral measurements were averaged and are graphed in Figure 3. The peaks observed at ~670 and ~740 nm in Figure 3 are attributed to source normalization artifacts due to a poor signal-to-noise ratio at the spectral extremities of our spectrophotometer (see Figure S5 in the Supporting Information for the emitted spectrum from the xenon light source). A MATLAB script (Supporting Information) individually calculated the peak shift and FWHM for each spectral measurement, and the values were averaged to obtain peak shift and FWHM statistics.

Two important optical characteristics for visual detection are the peak shift and change in FWHM upon assembly and disassembly. Peak shift upon assembly is defined as $\Delta\lambda_{peak} = \lambda_{peak,core+sat.} - \lambda_{peak,core}$ and is depicted on the x-axis of Figure 4a. The maximum attained assembly red shifts were approximately ~70 nm for all combinations of 50 and 30 nm AuNPs. Thirty nanometer satellites consistently produced the largest peak shift of all the satellite sizes. This behavior seems contrary to intuition as 50 nm satellites cause a larger structural change than 30 nm satellites. Limited

streptavidin conjugation onto the larger 50 nm AuNPs may have resulted in fewer satellites capable of binding to the core particles. Next, the peak shift upon disassembly was analyzed and is depicted on the *x*-axis of Figure 4b. Combinations of 30 and 50 nm AuNPs provided the largest blue shift, with 30 nm core and 50 nm satellite assemblies causing a maximum shift of 48.3 nm. The investigation reveals that the assembly red shift is not completely reversible, which may be caused by nonspecific aggregation of the satellites to the substrate and/or irreversible core–satellite attachment. Overall, core–satellite combinations of 30 and 50 nm result in the largest spectral peak shifts. The findings of this analysis correlate well with previous theoretical simulations of core–satellite plasmon band red shifting due to interparticle dipole coupling and radiation damping.[10,28]

The second optical characteristic analyzed was the FWHM assembly broadening and disassembly narrowing properties of the nanoassemblies. Analysis of the FWHM is necessary to maximize the signal-to-noise ratio during biosensing as large FWHM increases may cause disassembly blue shifts to be indiscernible. The change in the bandwidth upon assembly, defined as $\Delta\text{FWHM} = \text{FWHM}_{\text{core+sat.}} - \text{FWHM}_{\text{core}}$, was a maximum, 75.9 nm, for the 50 nm core and 30 nm satellite assembly (Figure 4a). Other combinations of 30 and 50 nm AuNP produced ~56 nm in bandwidth broadening. During disassembly, 50 nm cores with 30 nm satellites obtained the maximum bandwidth narrowing (Figure 4b). Minimizing the bandwidth upon assembly and disassembly is essential such that only one color, a single peak, can be easily resolved by human eye for both cases. Thus optimal core–satellite combinations would lie in the lower right side of Figure 4a,b. However, our data reveal that shifts in peak position appear to be positively correlated to changes in bandwidth. These results coincide with recent findings that larger satellite sizes broaden the plasmon band when assembled onto core AuNPs.[28] This characteristic is mainly due to retardation effects as the nanoassembly size becomes significant in comparison to the wavelength of light. Radiation damping has been shown to be a large factor in the red shifts observed in the far-field scattering as nanoparticles increase in size.[26] Ultimately, larger satellite sizes should lead to greater changes in FWHM upon assembly and disassembly. Similar to the nanoassemblies' characteristics with regard to peak shift, 30 nm satellites consistently produced the greatest fluctuations in bandwidth for both assembly and disassembly.

TABLE 1. Figure of Merit for Core–Satellite Assemblies

	10 nm	0.10	0.05	0.01	0.07
satellite size	30 nm	0.26	**0.28**	0.10	0.08
	50 nm	0.37	**0.25**	0.09	0.03
		30 nm	50 nm	80 nm	100 nm
			core size		

In order to quantify the overall biosensing capability of each nanoassembly variation, we have proposed the use of a figure of merit (FOM) for detecting plasmon peak shifts[28]

$$\text{FOM} = \frac{\Delta\lambda_{\text{peak}}}{\langle\text{FWHM}\rangle}$$

where ⟨FWHM⟩ is the average of the two FWHM values. The FOM takes into account both the peak shift and plasmon bandwidth, quantifying the nanoassemblies' ability to provide a resolved and observable colorimetric change. The experimentally obtained FOM values are shown in Table 1 for the nanoassembly variations we have studied. The substrate with 30 nm cores and 50 nm satellites has the highest FOM value, 0.37. However, the small scattering cross section of a 30 nm core AuNP made this substrate very difficult to observe by the naked eye. The second and third nanoassemblies with the next highest FOM values, 50 nm cores with 30 and 50 nm satellite sizes, yielded spectacular color shifts for our given experimental setup (Figure 2). These two combinations of nanoassembly are optimal.

CONCLUSION

We have proposed an advancement upon the current suspension-based modality of colloidal biomolecular sensors that is better suited for on-chip diagnostic system integration while preserving the capability for diverse species detection. We present the fabrication of nanoassemblies self-assembled on a two-dimensional glass substrate, demonstrate the colorimetric functionality of biomolecular sensing *via* trypsin-mediated disassembly, and systematically analyze the optical detection properties of the substrate. A FOM was determined to quantify the visual resolution of the color change and nanoassemblies with 50 nm cores and either 30 or 50 nm satellites were concluded to be optimal. To the best of our knowledge, this plasmonic biosensor is the first self-assembled substrate that yields a structural color change directly at the site of disassembly. This new modality may enable a new generation of robust POC diagnostic devices with enhanced sensing capabilities.

METHODS

Nanoassembled Substrate Fabrication. Droplet immobilizers were prepared by cutting 1 in. × 1 in. squares of cured, 4 mm thick PDMS (Dow Corning) and punching a 20 mm circle through the center. One droplet immobilizer was placed in the middle of a 1 in. × 3 in. 3-aminopropyltriethoxysilane (APTES)-treated microscope slide (The Microscope Store). The slides were cleaned with a stream of nitrogen and immediately placed in a Petri dish. The

surface adhesion of the PDMS to the APTES-treated slide prevented liquid leakage and capillary remodeling due to surface dehydration. Gold colloid (800 μL, British Biocell International) at stock concentration was pipetted into the PDMS well and incubated at 4 °C for 18 h. The wells were then washed multiple times with DI water (Milli-Q). A 50 μg/mL solution of the biotinylated peptide, biotin-GGRGDGKGGC-OH (Chi Scientific), in 1× PBS buffer (Gibco, Invitrogen) was prepared. The peptide solution was pipetted (800 μL) into the PDMS well and incubated at 4 °C for 18 h. The wells were again washed with DI water. A 2 mM mPEG-SVA (M_W = 2 kDa, Laysan Bio) solution was prepared in 100 mM $NaHCO_3$ (pH 8.25, Sigma-Aldrich) and sonicated briefly.[29] The mPEG-SVA solution was then pipetted (800 μL) into the PDMS well and incubated at room temperature (25 °C) for 6 h. The wells were again washed with DI water. Finally, streptavidin-conjugated AuNPs were pipetted (800 μL) into the well and incubated at 4 °C for 12 h. The slides were then washed with DI water and stored at 4 °C before exposure to 0.25% trypsin-EDTA 1× (Gibco, Invitrogen).

Streptavidin Conjugation onto AuNPs. A modified version of a previous protocol was used.[30] A sodium borax buffer was prepared by titrating 10 mL of 200 mM H_3BO_3 (pH 5.4, Sigma-Aldrich) with 2 mM $Na_2B_4O_7$ (pH 8.9, Sigma-Aldrich) to a final pH 7.1 (~18 mL of 2 mM $Na_2B_4O_7$ was added). The pH of the buffer is essential as it must be above the isoelectric point of streptavidin (pI ≈ 5.0) such that streptavidin can displace the negatively charged citrate groups adsorbed on the surface the AuNPs, but not too high of a pH as excess salt ions from $Na_2B_4O_7$ will induce flocculation. One milliliter of 10, 30, and 50 nm AuNPs (stock concentration) was spun down at 14 000, 10 000, and 7000 rpm for 10, 8, and 5 min, respectively. The supernatant was discarded, and the particles were resuspended in an equal volume (1 mL) of 5 μg/mL streptavidin (SouthernBiotech) in the sodium borax buffer. The suspension was placed on a rocker for 15 min to allow physio-adsorption. The streptavidin-conjugated AuNPs were spun down again, and the supernatant was discard. The conjugated AuNPs were resuspended in DI water. A 1% w/v NaCl (Sigma-Aldrich) test was performed to ensure streptavidin conjugation. Conjugated AuNPs can withstand salt concentrations up to 2−3% before crashing out of solution.

Dark-Field Spectroscopy. The nanoassemblies were imaged in dark field with an inverted microscope (Carl Zeiss Axiovert 200) under illumination from a xenon light source (Karl Storz). The scattered light was collected by a 20× microscope objective (Carl Zeiss, LD Achroplan) with a numerical aperture (NA = 0.40) smaller than that of the Nikon DF dry condenser lens (NA = 0.80−0.95). The spectra were acquired with a Princeton Instruments Acton SP2300 using WinSpec, and images were taken with a true-color CCD (QImaging Micropublisher 3.3 RTV). All measurements were taken with the nanoassemblies immersed in DI water and at room temperature (25 °C).

Acknowledgment. J.W. gratefully acknowledges support from an NSF Graduate Research Fellowship. The authors acknowledge financial support from the National Institutes of Health (NIH) Nanomedicine Development Center for the Optical Control of Biological Function (Grant No. 3PN2 EY01824), Center for Nanostructured Materials and Technology (CNMT), National Academies Keck Futures Initiative funding (Grant No. NA-KFI Nano09), DARPA MF3 (Award No. HR0011-06-10050), and DARPA SERS S&T Fundamental Program under LLNL subcontract (Grant No. B573237). We thank N. Choudhary for her early contributions to the project.

Supporting Information Available: Details concerning the scattering properties of various sized AuNPs, sample standard deviation measurements for peak and FWHM measurements, microfluidic device bonded onto core−satellite substrate, emission spectra of xenon light source, AuNP fabrication data, predicted detection times for physiologically relevant biosamples, and MATLAB scripts for spectral data analysis. This material is available free of charge *via* the Internet at http://pubs.acs.org.

REFERENCES AND NOTES

1. Mirkin, C. A.; Letsinger, R. L.; Mucic, R. C.; Storhoff, J. J. A DNA-Based Method for Rationally Assembling Nanoparticles into Microscopic Materials. *Nature* **1996**, *382*, 607–609.
2. Nykypanchuk, D.; Maye, M. M.; van der Lelie, D.; Gang, O. DNA-Guided Crystallization of Colloidal Nanoparticles. *Nature* **2008**, *451*, 549–552.
3. Alivisatos, A. P.; Johnsson, K. P.; Peng, X.; Wilson, T. E.; Loweth, C. J.; Bruchez, M. P., Jr.; Schultz, P. G. Organization of `Nanocrystal Molecules' Using DNA. *Nature* **1996**, *382*, 609–611.
4. Loweth, C. J.; Caldwell, W. B.; Peng, X.; Alivisatos, A. P.; Schultz, P. G. DNA-Based Assembly of Gold Nanocrystals. *Angew. Chem., Int. Ed.* **1999**, *38*, 1808–1812.
5. Yao, H.; Yi, C.; Tzang, C. H.; Zhu, J.; Yang, M. DNA-Directed Self-Assembly of Gold Nanoparticles into Binary and Ternary Nanostructures. *Nanotechnology* **2007**, *18*, 015102.
6. Xu, X.; Rosi, N. L.; Wang, Y.; Huo, F.; Mirkin, C. A. Asymmetric Functionalization of Gold Nanoparticles with Oligonucleotides. *J. Am. Chem. Soc.* **2006**, *128*, 9286–9287.
7. Maye, M. M.; Nykypanchuk, D.; Cuisinier, M.; van der Lelie, D.; Gang, O. Stepwise Surface Encoding for High-Throughput Assembly of Nanoclusters. *Nat. Mater.* **2009**, *8*, 388–391.
8. Sadasivan, S.; Dujardin, E.; Li, M.; Johnson, C. J.; Mann, S. DNA-Driven Assembly of Mesoporous Silica/Gold Satellite Nanostructures. *Small* **2005**, *1*, 103–106.
9. Li, B.; Li, C. Y. Immobilizing Au Nanoparticles with Polymer Single Crystals, Patterning and Asymmetric Functionalization. *J. Am. Chem. Soc.* **2007**, *129*, 12–13.
10. Sebba, D. S.; Mock, J. J.; Smith, D. R.; LaBean, T. H.; Lazarides, A. A. Reconfigurable Core−Satellite Nanoassemblies as Molecularly-Driven Plasmonic Switches. *Nano Lett.* **2008**, *8*, 1803–1808.
11. Sonnichsen, C.; Reinhard, B. M.; Liphardt, J.; Alivisatos, A. P. A Molecular Ruler Based on Plasmon Coupling of Single Gold and Silver Nanoparticles. *Nat. Biotechnol.* **2005**, *23*, 741–745.
12. Elghanian, R.; Storhoff, J. J.; Mucic, R. C.; Letsinger, R. L.; Mirkin, C. A. Selective Colorimetric Detection of Polynucleotides Based on the Distance-Dependent Optical Properties of Gold Nanoparticles. *Science* **1997**, *277*, 1078–1081.
13. Liu, J.; Lu, Y. Fast Colorimetric Sensing of Adenosine and Cocaine Based on a General Sensor Design Involving Aptamers and Nanoparticles. *Angew. Chem., Int. Ed.* **2006**, *45*, 90–94.
14. Liu, J.; Lu, Y. A Colorimetric Lead Biosensor Using DNAzyme-Directed Assembly of Gold Nanoparticles. *J. Am. Chem. Soc.* **2003**, *125*, 6642–6643.
15. Jun, Y. W.; Sheikholeslami, S.; Hostetter, D. R.; Tajon, C.; Craik, C. S.; Alivisatos, A. P. Continuous Imaging of Plasmon Rulers in Live Cells Reveals Early-Stage Caspase-3 Activation at the Single-Molecule Level. *Proc. Natl. Acad. Sci. U.S.A.* **2009**, *106*, 17735–17740.
16. Hirsch, L. R.; Jackson, J. B.; Lee, A.; Halas, N. J.; West, J. L. A Whole Blood Immunoassay Using Gold Nanoshells. *Anal. Chem.* **2003**, *75*, 2377–2381.
17. Myers, F. B.; Lee, L. P. Innovations in Optical Microfluidic Technologies for Point-of-Care Diagnostics. *Lab Chip* **2008**, *8*, 2015–2031.
18. Anker, J. N.; Hall, W. P.; Lyandres, O.; Shah, N. C.; Zhao, J.; Van Duyne, R. P. Biosensing with Plasmonic Nanosensors. *Nat. Mater.* **2008**, *7*, 442–453.
19. Zhao, W.; Ali, M. M.; Aguirre, S. D.; Brook, M. A.; Li, Y. Paper-Based Bioassays Using Gold Nanoparticle Colorimetric Probes. *Anal. Chem.* **2008**, *80*, 8431–8437.
20. Charrier, A.; Candoni, N.; Liachenko, N.; Thibaudau, F. 2D Aggregation and Selective Desorption of Nanoparticle Probes: A New Method To Probe DNA Mismatches and Damages. *Biosens. Bioelectron.* **2007**, *22*, 1881–1886.
21. Ramseier, C. A.; Kinney, J. S.; Herr, A. E.; Braun, T.; Sugai, J. V.; Shelburne, C. A.; Rayburn, L. A.; Tran, H. M.; Singh, A. K.; Giannobile, W. V. Identification of Pathogen and Host-Response Markers Correlated with Periodontal Disease. *J. Periodontol.* **2009**, *80*, 436–446.
22. Tchetverikov, I.; Lohmander, L. S.; Verzijl, N.; Huizinga, T. W. J.; TeKoppele, J. M.; Hanemaaijer, R.; DeGroot, J. MMP Protein and Activity Levels in Synovial Fluid from Patients with Joint Injury, Inflammatory Arthritis, and Osteoarthritis. *Ann. Rheum. Dis.* **2005**, *64*, 694–698.

23. Brawley, O. W.; Ankerst, D. P.; Thompson, I. M. Screening for Prostate Cancer. *CA: Cancer J. Clin.* **2009**, *59*, 264–273.
24. Herr, A. E.; Hatch, A. V.; Throckmorton, D. J.; Tran, H. M.; Brennan, J. S.; Giannobile, W. V.; Singh, A. K. Microfluidic Immunoassays as Rapid Saliva-Based Clinical Diagnostics. *Proc. Natl. Acad. Sci. U.S.A.* **2007**, *104*, 5268–5273.
25. Turkevich, J.; Stevenson, P. C.; Hillier, J. A Study of the Nucleation and Growth Processes in the Synthesis of Colloidal Gold. *Discuss. Faraday Soc.* **1951**, *11*, 55–75.
26. Ross, B. M.; Lee, L. P. Comparison of Near- and Far-Field Measures for Plasmon Resonance of Metallic Nanoparticles. *Opt. Lett.* **2009**, *34*, 896–898.
27. Maier, I.; Morgan, M. R. A.; Lindner, W.; Pittner, F. Optical Resonance-Enhanced Absorption-Based Near-Field Immunochip Biosensor for Allergen Detection. *Anal. Chem.* **2008**, *80*, 2694–2703.
28. Ross, B. M.; Waldeisen, J. R.; Wang, T.; Lee, L. P. Strategies for Nanoplasmonic Core−Satellite Biomolecular Sensors: Theory-Based Design. *Appl. Phys. Lett.* **2009**, *95*, 193112.
29. Kim, Y.-P.; Oh, E.; Oh, Y.-H.; Moon, D. W.; Lee, T. G.; Kim, H.-S. Protein Kinase Assay on Peptide-Conjugated Gold Nanoparticles by Using Secondary-Ion Mass Spectrometric Imaging. *Angew. Chem., Int. Ed.* **2007**, *46*, 6816–6819.
30. Oliver, C. Immunocytochemical Methods and Protocols. In *Methods in Molecular Biology*; Javois, L. C., Ed.; Humana Press: Totowa, NJ, 1999; Vol. 115, pp 327−339.